CrossMark

Benchmarking PGAA, in-beam NAA, reactor-NAA and handheld XRF spectrometry for the element analysis of archeological bronzes

Boglárka Maróti[1] · Zsolt Révay[2] · László Szentmiklósi[1] · Krzysztof Kleszcz[2,3] · Dénes Párkányi[1] · Tamás Belgya[1]

Abstract
Novel detection strategies were developed to improve the PGAA methodology in the analysis of bronze and brass objects. Instrumental neutron activation analysis and X-ray fluorescence were also involved in this study for comparison. The approach was tested on a set of IRMM-certified copper alloys. Reference values for the concentrations of four major additive components (As, Zn, Sn, and Pb) were compared with the results obtained by the involved methods. The bias observed between the reference Sn values and the initial PGAA results was successfully addressed by considering the interference of this line with low intensity copper prompt gamma peaks. In this report results are presented, and the analytical merits are compared.

Keywords PGAA · In-beam activation analysis · INAA · XRF · IRMM BCR-691 · Certified reference copper alloys

Introduction

The cultural-heritage community is deeply interested in the non-destructive chemical analysis of ancient copper alloys [1, 2] to investigate their provenance and manufacturing technology. The widespread analytical techniques, such as energy dispersive X-ray fluorescence (EDXRF), particle induced X-ray emission (PIXE), laser ablation inductively coupled plasma mass spectrometry (LA-ICP-MS), scanning electron microscopy combined with energy-dispersive X-ray spectroscopy (SEM–EDX), laser-induced breakdown spectroscopy (LIBS) all provide analytical information only about a small spot on the surface, unless cross-section samples are taken. Hence, if contamination, surface corrosion or patina are present on the object, the data by these methods may not be representative to the entire object. This can lead to large variation and/or bias of the measured concentrations, and finally to a wrong archaeometric interpretation. However, they proved to be useful to assess, for instance, the required restoration techniques [3, 4]. The representative bulk alloy composition is often obtained by means of destructive chemical analytical methods, such as ICP-MS, ICP-OES or ICP-AAS [2, 3, 5], but invasive chemical analysis is permitted only if non-destructive methods are inapplicable [1, 6].

Prompt Gamma Activation Analysis (PGAA) was used for the non-destructive bulk analysis of valuable artefacts already in the late nineties [7], using internal monostandard approach. The k_0 standardization, the spectroscopic library [8–10] and the reliable spectrum-evaluation procedure gave rise to the applications of PGAA for geology, material-science and archaeology samples, including metals [11, 12].

When the matrix contains elements with high neutron-capture cross section, such as copper, the detection of minor and trace components by PGAA is not always successful [13, 14]. Our aim with the present study was to improve the analytical merit of PGAA in alloy analysis by using tailored irradiation and detection techniques, such as

✉ Boglárka Maróti
maroti.boglarka@energia.mta.hu

1 Nuclear Analysis and Radiography Department, Centre for Energy Research, Hungarian Academy of Sciences, Konkoly-Thege Miklós Street 29-33, Budapest 1121, Hungary

2 Forschungsneutronenquelle Heinz Maier-Leibnitz (FRM II), Technische Universität München, Lichtenberg Str. 1, 85747 Garching, Germany

3 State Higher Vocational School in Tarnow, Mickiewicza 8 Str., 33-100 Tarnów, Poland

the high-resolution PGAA [13], high-flux PGAA [15], PGAA with a γ-ray attenuator [16] and compare their performances with in-beam activation analysis [15]. Considering the widespread use of reactor-based instrumental neutron activation analysis (INAA) [17] and handheld X-ray fluorescence spectrometry (XRF), these methods served here as references. With the single exception of INAA, all other tested approaches are non-destructive, hence applicable to such precious samples.

To avoid any bias due to the potential inhomogeneity or surface-bulk composition difference, the IRMM BCR-691 certified reference materials (CRM) were used for comparison [18] instead of real artefacts.

Materials

IRMM BCR certified reference materials

It is a set of five copper alloys (labelled as A–E), intended mainly for calibration [19] or quality control [20, 21] of XRF instruments, representing the common ancient bronze and brass types. When using micro beam methods on the BCR-691 CRMs, the recommendations regarding the minimum mass or spot size must be strictly followed [22] due to the micro-scale inhomogeneities, as reported by Constantinides et al. [18] and Arana et al. [23]. When using PGAA, these inhomogeneities have no effect on the analytical results as the analyzed volume exceeds several mm^3.

Quaternary alloy (A)

This simulated alloy represents the latest ancient alloy-type from this set of CRMs [22]. Quaternary alloy consists of four different metals, in this case: Cu, Pb, Sn and Zn. This is a typical alloy-type of the Roman Age [22, 24], mostly made of recycled materials.

Brass (B)

The second latest alloy type from the BCR set is the zinc containing copper alloy, the brass. The beginning of deliberate production of brass is dated around the first Millennium BC [25]. Besides Cu, the matrix component and Zn, the main alloy component, this CRM contains 2 m% (mass percent) tin.

Arsenic-copper (C)

This early type of copper-alloy was produced already from the forth Millennium BC [26]. Arsenic was probably not always an intentional addition, as copper oxide ores often contain a mixture of primary sulphides, in which the arsenic quantity was dependent on the proportion of the arsenic sulphide minerals [26]. Arsenic in certain amounts, similarly to tin, influences positively on the properties of the casting, but due to its volatile and toxic nature, arsenic-copper was not used more extensively later [27].

Lead-bronze (D)

Lead, as an alloying element is known from the Late Bronze Age (Hallstatt B period, 1000–800 BC). Its importance increased during the Iron Age (800–100 BC), especially with the appearance of the ternary alloys in the Celtic metalwork culture [28].

Tin-bronze (E)

Tin was intentionally added to copper to make its physical properties and moldability better. The alloy of copper and tin is called bronze. By the appearance of this alloy-type, a new prehistoric period started, namely the Bronze Age. At lower concentrations (1–4 m%), tin improves the malleability, hardness and tensile strength of the alloy. However, the majority of the Bronze Age bronzes contains tin in about 8–12 m% [27].

Experimental and data analysis

PGAA-based detection strategies

1. *Conventional PGAA* measurements were carried out at the PGAA station of the Budapest Neutron Centre (BNC) using a 27% HPGe detector with BGO Compton-suppressor and a cold-neutron beamline with a thermal equivalent neutron flux of 9×10^7 cm^{-2} s^{-1} [29].
2. *High-flux PGAA* measurements (with the flux of 2×10^8 cm^{-2} s^{-1}) were performed at the FRM II reactor at the Heinz Meier-Leibnitz Zentrum (MLZ) Garching, Germany [30] with a 60% efficient, Compton-suppressed HPGe detector in order to see whether the analytical results can be improved just by making the counting statistics better.

   In addition to these standard cases, we used the following modifications to the Budapest and Garching PGAA setups:
3. *PGAA with a γ-ray attenuator* between the sample and the detector was used to suppress the high count rate from the low-energy gamma rays of copper. The intensity of the low-energy peaks can be reduced with this filter by a factor of 75–80 or more, relative to the 7915 keV prompt-gamma line of copper, while—by maintaining the same overall count rate limited by the

counting electronics—the specific count rates of the high-energy peaks, including those from the minor components, could be enhanced. Similar gamma-ray attenuation method was applied successfully on samples with high boron content [16] and tested on two pieces of certified bronze alloys [14]. In our case, a 10-mm thick lead plate was used, whose gamma-ray attenuation as a function of energy was carefully characterized.

4. *High-resolution PGAA* is based on the use of a planar low-energy germanium (LEGe) detector equipped with a BGO Compton-suppressor. It can detect the elements with intense low-energy lines, typically below 500 keV where this detector type has a significantly better resolution than the typically used co-axial semiconductor detectors. Its efficiency falls quickly towards the high energies, thus, the vast amount of analytically unuseful counts in the continuum region (1–5 MeV), related to the Compton-plateaus of the high-energy prompt-gamma lines and the unresolvable closely-spaced capture-cascade lines are inherently not registered [13]. Using this configuration, we focused on the more selective identification and evaluation of the most prominent analytical lines, making some so-far unreliable analytical peaks useful.

The spectrum evaluation was performed in all cases using the Hypermet-PC [31] and PeakFit programs [32], whereas the concentration calculation was carried out with the Excel package ProSpeRo [33, 34].

In-beam activation analysis

The idea of in-beam activation analysis, i.e. the combination of a PGAA with off-line gamma-counting was introduced in 2008 [35]. Even oversized samples with dimensions exceeding the size of the irradiation capsules of INAA can be analyzed this way. The samples are irradiated in a horizontal channel or in a guided-neutron beamline preferably combined with a PGAA measurement. The in-beam activation is followed by a separate off-line counting step using an HPGe detector in a low-background chamber [15], just like in INAA. The lower flux compared to that of a vertical irradiation channel is at least partly compensated by the use of more massive samples. As the samples might be larger than the beam cross section, the irradiated mass is not known exactly. The element mass ratios from the decay measurement can be scaled to an absolute concentration using an internal standard also determined with PGAA.

The advantage of a cold-neutron beam for in-beam activation analysis is that all nuclides strictly follow the 1/v law and epithermal activation is completely avoided, so calculation is simple. But, if an element with high resonance integral (e.g. As, Ag, Sn, Sb) [36] is to be quantified, the irradiation can take place (even as a byproduct of an imaging experiment) at a horizontal thermal beam port of a reactor, such as the RAD station of BNC [37], where the more energetic neutrons and the larger beam dimensions allow the activation of objects up to 10–15 cm size with a good representativity, but in exchange, the activation calculations are more complicates.

The irradiation times at cold-neutron PGAA beamline of MLZ were 2–5 min with a flux of 3×10^{10} cm^{-2} s^{-1} [30]. Subsequently, three off-line decay measurements were performed on each sample, the first immediately after the irradiation, the second after 30–60 min of cooling time, and the third one after 2–3 days. The concentration calculation relied on the k_0 database [36, 38] and on the general formulae of INAA simplified to subthermal activation, containing the saturation (S), decay (D) and counting (C) factors to account for the growth of the radionuclide during activation, as well as its decay during cooling and counting times. The formula used for concentration calculation is partly derived from Eq. (2) of [33] used for calculation of masses in a prompt gamma spectrum. Equation (1) contains the SDC factors as well, as during the decay counting the gamma rays of the radioactive daughter nuclei are measured.

$$\frac{A}{\varepsilon t} = n\sigma\Phi SDC \tag{1}$$

where n is the number of target atoms in the analyzed volume and sigma is the thermal neutron capture cross-section, Φ is the thermal-equivalent neutron flux, ε is the counting efficiency, t is the measurement time.

k_0 instrumental neutron activation analysis

Due to the limited volume of the irradiation capsule used in a vertical channel, destructive sampling was needed for INAA measurements, which would not necessarily be possible for real artefacts. Therefore, these measurements were carried out as a final step of the work. In order to meet the minimum sampling requirement of the IRMM standard (100 mg, or XRF spot size of 5 mm in diameter) and the study on the certification procedure [18], approximately 100 mg from each copper alloy standard was taken. The sub-samples were cleaned with alcohol, dried, precisely weighed, loaded into polyimide carrier capsules together with the Au, Fe and Zr flux monitors. The samples were irradiated for 180 s using the fast-rabbit irradiation channel where the neutron flux is 5.3×10^{13} cm^{-2} s^{-1}, and is well thermalized ($f \approx 37$) [17], so the best detection limits were expected from this technique. The irradiated samples were cooled and measured twice in a low-background counting chamber. The first decay measurements took place after

7 days. The acquisition times were set to 40 min. The second gamma counting took place 66 days after the irradiation, when all short-lived radionuclides had decayed away, reducing the general Compton-background. The acquisition time was 4 h for each sample. The counting system consisted of an Ortec 55% HPGe detector, an Ortec DSPEC 502 spectrometer operated in zero-dead-time (ZDT) mode, and a low-level counting chamber made of pre-WW2 iron. For the evaluation of the NAA data we applied the k_0 approach using the Hyperlab 2013 [39] and Kayzero for Windows 3 [40]. The neutron self-shielding was corrected for as described in Ref [41].

X-ray fluorescence spectrometry

The XRF spectrometry measurements were completed using an Innov-X Delta Premium type handheld XRF analyzer. This equipment is designed for the (on-site) analysis of contemporary metal alloys, but it is suitable for the analysis of other materials (e.g. ores, soils) as well where matrix-specific calibration is available. Such device is often used in archaeometry due to its simplicity and low analysis cost.

In our study, its Alloy Plus settings were applied, even though this mode of the instrument does not report the As-content, an indicative constituent of the ancient copper-based alloys. The X-ray spot size was 3 mm in diameter ($\sim$ 7 mm^2), and five measurements were statistically averaged. Each measurement took 30 s, and elemental-composition calculation (based on the Fundamental Parameters approach) was done by the built-in software of the device. The other main advantage of the handheld XRF analyzer is that, similarly to PGAA, it does not require any sample preparation either.

Revised interference correction for PGAA

In a usual bronze PGAA spectrum, only the three most intense tin peaks can be detected: at 1293.5, 1171.3 and 1229.6 keV, with relative intensities of 100, 65.6 and 50.3%, respectively. The minor copper lines close to these tin lines have relative intensities of about 1–4% (Table 1). Next to the 1229 keV tin line we identified a weak copper peak at 1231.756(61) keV [10].

The partial gamma-ray production cross section of 1229.6-keV tin line has a cross section of 0.0673(13) b, while the 1231.8-keV copper line has 0.0102(8) b. Considering that the bronze contains 20–60 times more Cu atoms than Sn (see Table 2), the count rates of the overlapping peak pairs become comparable. At lower tin concentrations, the count rate of the copper peak can be 6–20 times more than that of the close-lying tin peak.

Table 1 Prompt gamma peaks of tin and copper located between 1171 and 1320 keV [10]

Element	Energy (keV)	Unc. energy (keV)	σ_γ
Sn	1171.282	0.059	0.0879(13)
Sn	1229.644	0.059	0.0674(13)
Cu	1231.756	0.061	0.0102 (8)
Cu	1241.715	0.079	0.0346(12)
Sn	1293.53	0.059	0.1340(21)
Cu	1320.037	0.042	0.0219(8)

Table 3 lists the observed bias between the reference values and the concentrations obtained with the uncorrected standard PGAA methodology. It was realized that the magnitude of the bias is in anti-correlation with the Sn content, i.e. the cause of this bias is not the incorrect cross section value, but the inappropriate interference correction. The use of the standard interference correction library that contains prompt gamma lines down to 1% relative intensity [10, 33], is proven to be insufficient in this scenario. An extended version, containing additional two hundred Cu peaks with lower intensities, was created and applied to overcome the problem.

The newly introduced interference correction practice was tested on a tin-bronze European Reference Material (ERM), ERM®-EB374, too. It contains 7.6 m% tin with negligible amounts of Ag, Fe, Mn, Ni, Pb, Zn, at far below 50 ppm quantities. Before the correction, 9.6 $\pm$ 0.3 m% tin content was determined, while after the proper interference correction, the tin content became 7.9 $\pm$ 0.3 m%. The Sn/Cu ratios are 0.107 $\pm$ 0.003, 0.0824 $\pm$ 0.0014 and 0.0859 $\pm$ 0.0026 for the uncorrected result, the reference values and for the adequately corrected PGAA result, respectively.

For the accurate quantification of low-intensity copper lines, high-purity copper sheets with the thicknesses of 7 μm and 1 mm were analyzed (99.9% purity Cu 131710, ADVENT R. M. Ltd.). In order to convert the relative intensities of these low-intensity gamma lines to partial gamma-ray production cross sections (σ_γ), copper (II) chloride dihydrate was measured for standardization. The partial gamma-ray production cross sections were calculated according to Eq. (8) in Ref [9].

At 1171.345(54) and 1293.868(67) keV, low-intensity prompt peaks of Cu were confidently identified (see Fig. 1). The elemental spectra of Cu and Sn with appropriate weighting factors representing different mass fractions of Sn, were superimposed to illustrate the overlap at 1171.3 keV. In case of a 2 m% Sn content, the weak copper peak contributes to the area of 1171.3-keV peak by 50%, being the reason of the observed positive bias.

Table 2 Cu–Sn atomic ratios calculated into mass percentage unit and the produced analytical signal

Sn:Cu atomic ratio	Sn mass %	Cu mass %	Analytical signal (ratio) Cu/Sn
1:1	65	35	0.15
1:5	27	73	0.76
1:10	16	84	1.5
1:15	11	89	2.3
1:20	9	91	3
1:40	4.5	95.5	6.1
1:50	3.6	96.4	7.6
1:100	1.8	98.2	15.2

Table 3 Reference values for tin in the copper alloys compared to the conventional PGAA results (without the advanced correction detailed in the text)

Alloy	Tin mass percent				
	Reference value	STD Ref. (k = 2)	PGAA	PGAA STD (k = 2)	PGAA/reference value
Arsenic-copper (BCR-C)	0.202	0.01	ND		
Brass (BCR-B)	2.06	0.035	3.4	0.4	1.65
Tin-bronze (BCR-E)	7	0.3	9.8	0.8	1.40
Quaternary bronze (BCR-A)	7.16	0.105	7.5	0.9	1.05
Lead-bronze (BCR-D)	10.1	0.4	11.5	0.8	1.14

Note that in case of two mass percent tin content the bias is more than 50%
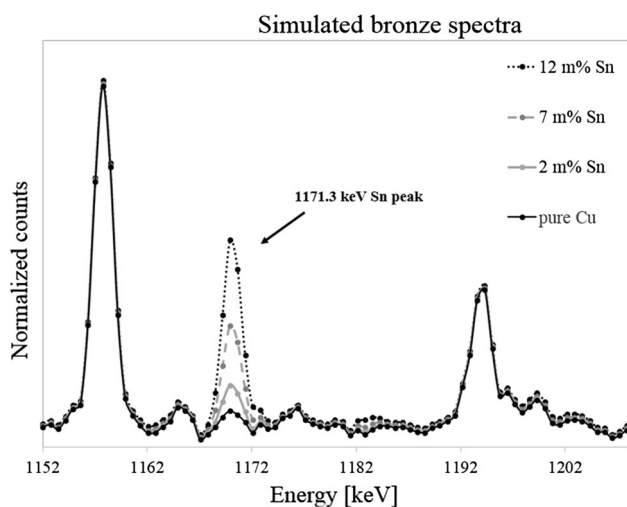
Fig. 1 Calculated bronze PGAA spectra with different tin mass fractions. The peak areas are normalized to the copper matrix peaks

The calculated partial cross section values for 1171- and 1293-keV Cu lines are 0.00126(13) and 0.00165(13) barn, respectively. These interferences were correctly taken into account during the concentration calculation stage. The summary of results with the revised tin concentrations is detailed later in the Table 4.

Results

Quaternary alloy

The four major constituents of the Quaternary alloy, Cu, Pb, Sn and Zn are all above 1 m% quantity, they could be quantified by all the methods involved in this study, except lead. Pb was not detected by INAA and in-beam NAA, since lead has no detectable radioactive daughter nuclide. Pb has a single prompt-gamma line at 7368 keV with low neutron capture cross section. High-resolution PGAA has orders of magnitude lower efficiency above 2000 keV, so this lead peak could not be detected using this setup. Except for attenuated PGAA and handheld XRF, arsenic content was analyzed with all methods within uncertainty margin. Note, that attenuated PGAA is not sensitive for the low-energy gammas on purpose. The poor sensitivity for arsenic is not the feature of the XRF method, but the weakness of the handheld device's embedded evaluation software. As, Ni and Sb can provide valuable information about the used ores during the production of the real ancient alloys. As the Ni and Sb were added to the mixture during the production of the simulated alloys, it can be concluded, that high-resolution PGAA, in-beam NAA, INAA and XRF methods are essential in the analysis of Sb. Nickel was detected with conventional and attenuated

Table 4 Results of the quaternary alloy, brass, arsenic copper, lead-bronze and tin-bronze samples (BCR-691 A–E) using different PGAA settings and a handheld XRF device in m% unit. The certified reference and informative values are marked with bold and italic letters, respectively. < DL implies if the element was below the detection limits under the given measurement conditions. N/A indicates if an element can not be detected due to methodological or nuclear physics reasons

Quaternary bronze (BCR-A)

	Ref values	±	NAA [23]	±	PIXE [23]	±	PGAA	±	Attenuated PGAA	±	High resolution PGAA	±	In-beam NAA	±	INAA	±	XRF	±
		k = 2		k = 2		k = 2	k = 2											
Cu	*Matrix*						76	0.9	77	0.8	**		**					
As	**0.194**	0.10	0.190	0.011	0.165	0.069	0.21	0.02	ND*		0.17	0.007	0.188	0.006	0.185	0.008	N/A	
Pb	**7.9**	0.7	N/A		8.12	1.4	8	1	7	0.6	N/A		N/A		N/A		8.1	0.6
Sn	**7.16**	0.21	6.92	0.42	6.78	1.1	7.1	0.26	7.9	0.3	8.6	0.3	8.3	0.4	6.4	0.5	7.1	0.1
Zn	**6.02**	0.22	6.22	0.35	6.06	1.0	6.8	0.3	6.0	0.3	6.6	0.3	6.3	0.4	5.7	0.2	5.7	0.2
Sb	*0.5*		0.514	0.029	0.44	0.07	ND		ND*		0.63	0.04	0.490	0.009	0.46	0.02	0.46	0.01
Ni	*0.1*						0.10	0.008	0.11	0.007	< DL		N/A		< DL		0.095	0.008
Mn	*0.2*						0.280	0.009	0.17	0.1	0.21		0.205	0.007	N/A		0.178	0.007
Fe	*0.2*						< DL		< DL		< DL		N/A		N/A		0.245	0.007
Ag	No data						< DL		N/A		0.013	0.001	N/A		0.011	0.002	< DL	

Brass (BCR-B)

	Ref values	±	NAA [21]	±	PIXE [21]	±	PGAA	±	Attenuated PGAA	±	High resolution PGAA	±	In-beam NAA	±	INAA	±	XRF	±
		k = 2		k = 2		k = 2	k = 2											
Cu	*Matrix*						81	0.6	81		**		**					
As	**0.099**	0.010	0.0989	0.0057	0.112	0.056	0.09	0.04	N/A		0.080		0.097	0.008	0.082	0.005	N/A	
Pb	**0.39**	0.04	ND		0.39	0.13	< DL		< DL		N/A		N/A		N/A		0.55	0.02
Sn	**2.06**	0.07	2.05	0.15	2.02	0.31	2.0	0.13	2.2	0.1	< DL		2.1	0.2	1.9	0.3	2.08	0.07
Zn	**14.8**	0.05	15.6	0.8	14.8	2.3	15	0.6	15	0.7	14.4		15.1		14.6	0.5	14.8	0.5
Sb	–		0.00121	0.00012	No data		< DL		N/A		< DL		< DL		0.0014	0.0002	< DL	
Ni	*0.2*						0.27	0.015	0.24	0.01	< DL		N/A		< DL		0.21	0.01
Mn	*0.4*						0.49	0.04	0.37	0.02	0.47		0.41	0.01	N/A		0.32	0.06
Fe	*0.5*						0.57	0.05	0.48	0.05	< DL		N/A		N/A		0.52	0.01
Ag	No data		No data		No data		< DL		N/A		0.012	0.008	N/A		0.012	0.002	< DL	

Table 4 continued

	Ref values	±	NAA [23]	±	PIXE [23]	±	PGAA	±	Attenuated PGAA	±	High resolution PGAA	±	In-beam NAA	±	INAA	±	XRF	±
Arsenic–copper (BCR-C)																		
Cu	*Matrix*	k = 2	k = 2		k = 2		95		95		**		**					
As	**4.6**	0.27	4.6	0.26	6.49	1.02	5.0	0.4	4.6	0.4	4.8		4.6	0.3	4.7	0.2	N/A	
Pb	**0.175**	0.014	ND		ND		< DL		< DL		N/A		N/A		N/A		0.37	0.04
Sn	**0.202**	0.029	0.205	0.035	0.24	0.06	0.39	0.05	< DL		< DL		< DL		< DL		0.22	0.03
Zn	**0.055**	0.005	0.0606	0.0075	0.058	0.034	< DL		< DL		< DL		< DL		0.054	0.014	< DL	
Sb	*0.5*		0.478	0.027	0.50	0.09	< DL		N/A		0.6		0.54	0.1	0.46	0.02	0.49	0.03
Ni	*–*						< DL		< DL		< DL		N/A		< DL		< DL	
Mn	*0.2*						0.190	0.005	< DL		0.30		0.201	0.015	N/A		0.15	0.05
Fe	*0.2*						< DL		< DL		< DL		N/A		N/A		0.19	0.02
Ag	*No data*		No data		No data		< DL		N/A		< DL (200 ppm)		N/A		0.013	0.001	< DL	

	Ref values	±	NAA [23]	±	PIXE [23]	±	PGAA	±	Attenuated PGAA	±	High resolution PGAA	±	In-beam NAA	±	INAA	±	XRF	±
Lead–bronze (BCR-D)																		
Cu	*Matrix*	k = 2	k = 2		k = 2		79		82		**		**					
As	**0.285**	0.022	0.289	0.016	0.271	0.094	0.34	0.03	N/A		0.25		0.277	0.02	0.27	0.01	N/A	
Pb	**9.2**	0.17	ND		9.5	2.1	10	1.3	7.0	0.7	N/A		N/A		N/A		10.9	0.6
Sn	**10.1**	0.8	10.3	0.6	9.79	1.53	9.9	0.35	10.1	0.3	11.0		< DL		9.1	0.5	9.65	0.26
Zn	**0.148**	0.024	0.157	0.010	0.21	0.08	< DL		< DL		< DL		< DL		0.14	0.01	< DL	
Sb	*0.3*		0.321	0.018	0.233	0.038	< DL		N/A		0.19		0.291	0.02	0.27	0.01	0.276	0.015
Ni	*0.3*						0.32	0.02	0.34	0.02	< DL		N/A		< DL		0.285	0.008
Mn	*0.1*						< DL		0.22	0.02	0.16		0.104	0.01	N/A		0.06	0.04
Fe	*0.1*						< DL		< DL		< DL		N/A		N/A		0.061	0.003
Ag	*No data*		No data		No data		< DL		N/A		0.018		N/A	0.002	0.011	0.001	< DL	

Table 4 continued

Tin-bronze (BCR-E)

	Ref values	±	NAA [23]	±	PIXE [23]	±	PGAA	±	Attenuated PGAA	±	High resolution PGAA	±	In-beam NAA	±	INAA	±	XRF	±
Cu	Matrix	k = 2		k = 2		k = 2	91	k = 2	92		**		**					
As	**0.194**	0.02	0.196	0.011	0.24	0.05	0.17	0.02	N/A		0.15	0.007	0.195	0.006	0.213	0.009	N/A	
Pb	**0.204**	0.018	ND		ND		<DL		<DL		N/A		N/A		N/A		0.29	0.02
Sn	**7.0**	0.6	6.90	0.43	7.32	1.18	7.8	0.3	6.7	0.2	6.3	0.3	6.4	0.4	6.7	0.5	7.30	0.08
Zn	**0.157**	0.025	0.169	0.011	0.15	0.12	<DL		<DL		<DL		<DL		0.15	0.02	<DL	
Sb	0.7		0.732	0.041	0.65	0.11	<DL		N/A		0.60	0.09	0.71	0.01	0.62	0.02	0.68	0.05
Ni	0.5						0.53	0.02	0.52	0.02	<DL		N/A		0.4	0.1	0.47	0.01
Mn	0.3						0.38	0.02	0.41	0.02	<DL		0.299	0.008	N/A		0.27	0.04
Fe	0.3						<DL		<DL		<DL		N/A		N/A		0.327	0.014
Ag	No data		No data		No data		<DL		N/A		0.018	0.001	N/A		0.013	0.001	<DL	

Reference and informative values together with NAA and PIXE results from previous studies are also involved [18, 22, 23]

** From conventional PGAA (relative)

PGAA and with XRF. Silver content was observed using high-resolution PGAA and INAA. As no information on silver addition in the CRM is available, this element is considered as a component in one of the metal powders.

Both polished (front) side and flattest part of the rear side of the CRMs were measured with handheld XRF. Table 4 contains the XRF results of the measurements carried out on the polished side. The front and the rear side has a Pb content of 8.1 ± 0.6 m% and 6.4 ± 0.5 m%, respectively, i.e. they showed more than 20% difference in lead content.

Brass

Tin was successfully determined with conventional and attenuated PGAA, using the proper interference corrections. Due to the detector efficiency, Sn could not be reported by high-resolution PGAA. Using in-beam NAA and off-line counting measurements, tin could be determined via its Sn-123m radionuclide. The determined concentrations agreed within one sigma.

Pb contents on the polished and the rear side agreed within uncertainty in case of the handheld XRF results. However, the observed Pb concentrations here were 25% above the reference value. This can be the consequence of the low Pb content (0.39%), and the arsenic content (0.099%) together.

Arsenic-copper

This type of copper alloy could be analyzed successfully with all our techniques (except for the As content by XRF). The only hindering fact was that in addition to arsenic and copper, the remaining low amount of Zn, Sn, Pb content could be only detected by XRF. Zn was reported by NAA, which requires destructive sampling.

As for XRF, the 50% bias from the reference value, and the 20% difference between the lead content of the two sides can partly be attributed to the high arsenic content (as an interfering element).

Lead-bronze and tin-bronze

If our specimen is lead-bronze or lead-containing tin bronze, besides conventional PGAA, PGAA with γ-ray attenuator and XRF can be methods of choice. Both lead and tin emit prompt gammas above 1 MeV as well as nickel, which, in real bronzes could be an impurity of the raw material [27].

While in case of a tin bronze (E) sample, the lead difference between the two sides was not observed in the XRF results, lead-bronze (D) showed the highest (30%) deviation in Pb concentrations (polished side: 10.9 ± 0.6 m%, rear side: 7.5 ± 0.4 m%).

In case of the Zn content of both the lead- and the tin-bronze, the XRF device erroneously calculates the detection limit for 600 ppm, yet, the Zn content of the alloys is higher than this value in both cases.

Discussion

When ancient metal artefacts from museum collections are analyzed, the turnaround time has also to be taken into consideration. Regarding the rapidity of the measurement, XRF cannot be challenged. Table 5 summarizes the characteristics and the time requirements of the applied methods. In case of conventional, attenuated and high-resolution PGAA, the samples are available 1–2 days after the irradiation. During in-beam activation analysis, a medium half-life nuclide, Sb-122 can be formed ($T_{1/2}$ = 2.7 days). Depending on the quantity of the Sb in the examined object and the irradiated mass, the artefact should be stored for more than 1 week in the laboratory in order meet the legal clearance level.

The conventional PGAA protocol reported As, Zn, Cu, Pb concentrations in agreement within the uncertainty margin to the certified value, while Sn was initially overestimated (with 5–65%). After revising the interference correction procedure, the results became compatible with the reference values.

From the additional elements (Sb, Ni, Mn, Fe) used during the production of the simulated copper-alloys [22], Ni was detected in all cases, while Mn in three samples and Fe only in the brass. Sb was not detected, being below the detection limit of the technique in this matrix.

PGAA with gamma-ray attenuator provided results with better statistics for elements having high-energy lines, such as Pb, Mn and Ni, thanks to the higher number of counts acquired in their respective peaks. For BCR-691 A and E, Sn was found to be an outlier when using this mode for the same reason as discussed above. After using the proper interference correction, the results became in line with the reference values. As a side effect of the gamma attenuator between the sample chamber and the detector, elements with strong low-energy gamma lines, such as Sb and As could not be detected.

In high-resolution PGAA mode, the LEGe detector has proven to be a useful addition to the standard PGAA system. The emerging high-intensity, often overlapping gamma lines in the low-energy range could be successfully resolved by the LEGe detector, in contrast to the conventionally used co-axial HPGe, whereas the high-energy part of the spectrum is suppressed due to the diminishing efficiency. Therefore, in addition to standard PGAA, the Sb content in the BCR-691 A, C, D and E samples became quantifyable using the low-energy gamma lines (Sample B does not contain Sb). In resolving multiplets, the peak-fitting patterns significantly differed from that of the PGAA, hence, targeted nuclear-data measurements were carried out to arrive at correct concentrations.

The high-flux PGAA reduced acquisition time but did not seem to be beneficial in case of copper alloys. The high count rate drives the electronics beyond their optimum performance, so the peak shapes are distorted and due to the increased chance of random coincidences the baseline in the spectrum is increased. For that reason, the results are not reliable and less precise than with the standard PGAA methodology.

To achieve the best detection limit for minor and trace components when using in beam NAA, it is required to wait until the radioactive nuclides of the matrix decay away. This is possible, if the radionuclides of the major constituents have shorter half-lives than the other

Table 5 Performance indicators of the different neutron-based analytical methods

Method	Collimator size	Actual irradiated mass (g)	Turnaround time of the whole analysis procedure
Conventional PGAA	10–24 mm^2	0.2–0.5 g	2–5 h
			(1–3 h of measurement, 1.5 h of spectrum evaluation)
Attenuated PGAA	24–44 mm^2	0.5–1 g	2–3 h
			(1–2 h of measurement, 0.5–1 h of spectrum evaluation)
High-resolution PGAA	24–44 mm^2	0.5–1 g	1–2 h
			(0.5–1.5 h of measurement, 0.5 h of spectrum evaluation)
In-beam activation analysis	150 mm^2	1–3 g	3–4 days
			(5 min of irradiation, total of 4 h gamma spectrometry measurements, 3–4 days cooling time, 0.5 h of spectrum evaluation per sample)
INAA	N/A	100 mg	15–70 days
			(180 s irradiation, 7 + 60 days of cooling time, 1–2 h of spectrum evaluation in batch mode)

components of interest. In case of in-beam activation analysis, unlike k_0-NAA, we need to detect the signal of the matrix components as well, because the other components (As, Sn, Sb, Zn, Mn) can be given only relative to a main constituent, and scaled to absolute masses via the Cu data from the standard PGAA.

The decay gamma-ray peaks that were found to be the most reliable for quantification are listed in Table 6.

Besides XRF, Instrumental neutron activation analysis could detect the most elements (with the exception of Pb, Fe and Ni), and its detection limits were the most advantageous. Mn was also not detected, as after the irradiation, the radioactivity was too high. Due to radiation protection reasons, the samples were stored in the depot of the fast rabbit system. The first measurement was carried out after 8–10 half-lives of Cu-64, and during this time the Mn-56 completely decayed away, as its half-life is 2.58 h.

The built-in software of the Olympus Delta Premium XRF analyzer does not report the arsenic concentration. To overcome this limitation, bAxil XRF spectrum fitting software [42] was used. The main difficulty is the simultaneous determination of arsenic and lead in the same sample, because the 10.5 keV arsenic Kα line strongly interferes with Pb Lα. Using bAxil software, lead and/or arsenic Kα was detected in all spectra. Arsenic Kβ was clearly visible in the arsenic copper alloy (BCR-C) and could be fitted in the spectra of the remaining alloys, too. The relative uncertainly of the arsenic Kβ peak is 11% in case of BCR-E. For BCR-A-B-D the Kβ peak area uncertainty is 30–35%. Lead Mα line could only be detected in case of BCR-A and D alloys, where the lead content is 7.9 and 9.2 m%, respectively. The handheld XRF measurements revealed significant compositional differences between the polished and the rear sides of the alloy discs, especially in the cases of Mn, Fe and Pb content. This effect was especially characteristic to the high-lead containing samples (A—quaternary alloy, D—lead bronze). In case of sample C, the signal of As is erroneously interpreted as Pb by the analysis software of

Innov-X, thus overestimating the Pb content to a large extent. The proper matrix calibration for arsenic and lead containing copper alloys is under way.

Detection limits

In case of NAA measurements the Kayzero for Windows 3 [40] software was used for the calculation of detection limit (DL). This program applies the detection limit as defined by Currie [43]. The DL values are calculated for all gamma-peaks present in the spectrum. A possible way to improve the detection limit of the elements of interest is to wait until the radioactive nuclide of the matrix component decays. If the matrix component has comparable or longer half-life than the other constituents, the searched peaks might be covered by the Compton plateau of the higher-energy, intense gamma peaks of the main component, thus worsening the detectability of the elements of interest.

While calculating the DL for the PGAA measurements, the peak-search algorithm settings of the applied spectrum fitting software [31, 32] needs to be taken into account [44] in addition to the Currie criterion [43]. Furthermore, the position of the peak in the prompt gamma spectrum (low-energy or high-energy range) has important influence on the minimum detectable area. The low-background regions with completely interference-free peaks are preferred. However, in the present study the detection limits might be worse because the spectra are complicated (type 2) [44]. The detection limits for conventional PGAA, attenuated PGAA and high-resolution PGAA are calculated using Eq. (23) of the Handbook of Prompt Gamma Activation Analysis [44], from selected intense, preferably interference-free prompt gamma peaks. In our case, t_{max} in Eq. (23) (which was referred to as the longest practicable measurement time and was defined in 100,000 s in Ref [44]) was replaced by the live-time of the individual measurements i.e. reasonable acquisition times (3000–9000 s).

Using in-beam activation analysis, the detection limit of a certain element is strongly dependent on the neutron flux, the irradiation time, the cooling time before measurement and the half-life of the formed radionuclides present in the sample. Note, that the detection limits can be slightly varied, if the measurement conditions change. The calculated detection limits are valid for 5 min of irradiation.

The detection limits of the handheld XRF were calculated by the built-in software of the device.

The detection limits of all different techniques used in this study are listed in Table 7, for a general overview.

It is valid for all the neutron-based methods, that the decisive factor is the element of interest relative to the copper amount.

Table 6 Peaks found to be useful in decay gamma-spectrometry following cold neutron irradiation

Energy (keV)	Half-life	Decay mode	Radioactive nuclide
511	12.7 h	β+	Cu-64
1345	12.7 h	β−	Cu-64
1039	307.2 s	β−	Cu-66
847, 1811, 2113	2.58 h	β−	Mn-56
439	13.7 h	IT	Zn-69m
559, 657, 1216	1.09 d	β−	As-76
160	2404 s	β−	Sn-123m
564	2.72 d	β−	Sb-122

Table 7 Detection limits (mass percents or µg/g noted as ppm) of possible minor and trace elements in different copper-based alloys

Element	INAA	In-beam activation analysis	Conventional PGAA	Attenuated PGAA	High-resolution PGAA	Handheld XRF
As	25–50 ppm	10–60 ppm	0.06–0.6%	1.1–10%	0.05–0.10%	N/A
Pb	N/A	N/A	3.0–6.0%	1.7–3.5%	N/A	200–800 ppm
Zn	90–150 ppm	0.3–1.2 m%	1.0–1.5%	1.6%	0.6%	400–2000 ppm
Sn	0.45–0.8%	0.23–0.3 m%	1.5–2.0%	0.5–1.0%	4.0%	150–700 ppm
Sb	3–6 ppm	5–20 ppm	0.8–1.0%	N/A	0.02–0.1%	200–500 ppm
Ni	N/A	N/A	20–400 ppm	20–300 ppm	0.2–0.7%	200 ppm
Mn	N/A	20–40 ppm	0.3–0.5%	0.1–0.3%	0.1–0.3%	50–100 ppm
Fe	N/A	N/A	0.4–0.6%	0.4–0.6%	0.4–0.6%	300 ppm
Ag	15–50 ppm	N/A	0.02–0.05%	N/A	50–100 ppm	200–300 ppm

N/A indicates if an element cannot be detected due to methodological or nuclear physical reasons

General assessment and recommended workflow

Different PGAA setups were tested in the analysis of bronze standards containing various amounts of As, Pb, Sn, Zn. Discrepancy was observed between the certified Sn values and the calculated concentrations in the case of PGAA-based methods. The copper interferences, causing the deviation, were successfully taken into account.

Thanks to different probing volumes of the neutron and X-ray based techniques, inhomogeneity problems, bias in the lead content between front and rear sides can be revealed even for a certified reference material. Lead inhomogeneity is an existing phenomenon in real bronzes as well. It is caused by the insolubility of lead in copper matrix [27]. Element misidentification of the handheld

XRF was also recognized, which must be taken care of during its routine applications.

The high-flux mode of PGAA could not yet be utilized routinely for bronze analysis due to instrumental problems, although it becomes practical when only a small amount of sample is available.

PGAA with lead gamma-ray attenuator shortened the required acquisition time and improved the precision of some poorly detectable elements, such as Sn, Pb and Ni, which have strong prompt gamma lines above 1 MeV. On the other hand, important peaks of Sb and As in the low-energy part of the spectrum are lost.

Additional Sb content could be determined using high-resolution PGAA, in-beam activation analysis, NAA and XRF method.
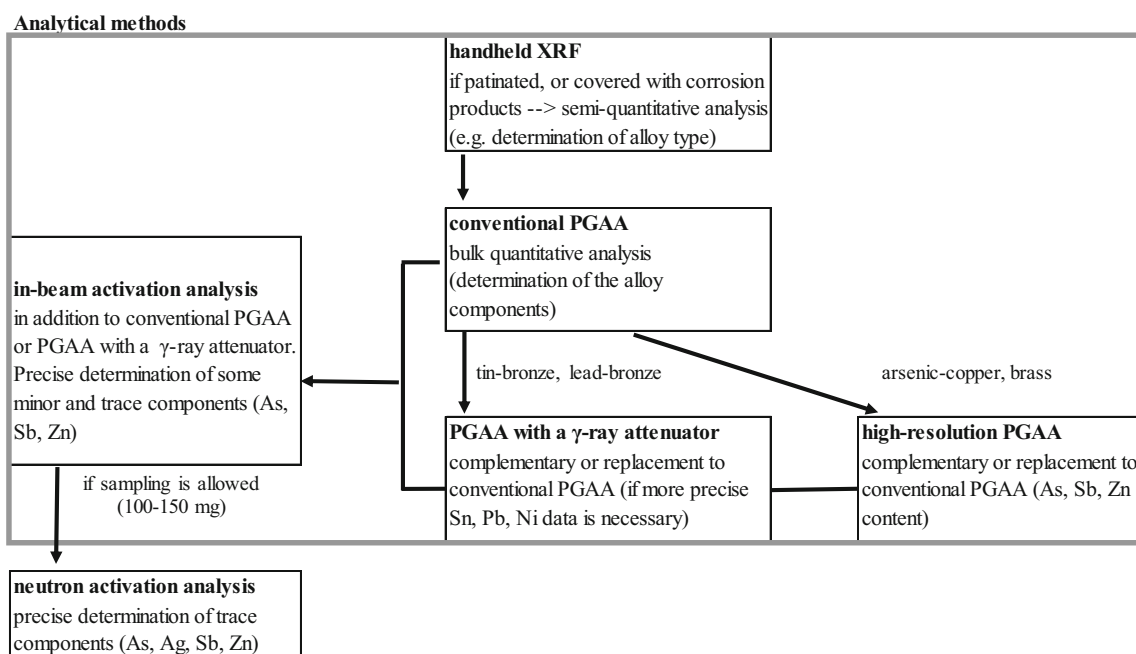

Fig. 2 Proposed measurements for the non-destructive bulk characterization of archaeological copper-alloys

The Ag content detected by NAA and high-resolution PGAA is probably the impurity of one of the used element powders.

The best combination of different PGAA setups to determine the most alloy components is gamma-attenuated PGAA—if the sample is not irregular and its thickness is limited to 2–3 mm—together with high-resolution PGAA or in-beam activation analysis. Lead and nickel can be determined using their high-energy gammas. Elements—undetectable using gamma attenuator—with low-energy gamma rays, all have short-lived radioactive nuclides, and can be analyzed with the help of in-beam activation analysis followed by off-line counting measurements. Furthermore, in-beam activation analysis offers more reliable peak identification and less spectral interference. One of the drawbacks of this method is that Pb cannot be analyzed, and due to the medium half-life radionuclides possibly forming, the sample should be kept in the laboratory for longer time.

The combination of these techniques improves the analytical merits of PGAA in bronze analysis, still in a non-destructive way. Figure 2 depicts a recommended measurement workflow. The completely non-destructive methods can be found within the gray frame.

Conclusions

We managed to develop specific irradiation and detection techniques capable of adding elements to the suite detected by the conventional PGAA measurement. With the introduction of advanced interference correction and considering even the low-intensity copper prompt gamma peaks, the previously overestimated tin concentrations became reliable even in case of low Sn amounts. Depending on the elements of interest, a combination of high-resolution PGAA (sensitive for As, Zn, Sb, Fe, Ag) and attenuated PGAA (sensitive for Pb, Sn, Ni, Mn, Fe) is recommended for the measurement of alloying elements and some impurities in copper-alloys. If the samples are of moderate size, conventional PGAA combined with off-line counting (e.g. in-beam activation analysis) is an optimum choice of methodology.

A proposed measurement protocol is appropriate for the analysis of ancient copper and copper-based objects that are not available for destructive sampling, or covered with altered surface layer, such as corrosion or patina.

References

1. Kiss V, Fischl KP, Horváth E, Gy Káli, Zs Kasztovszky, Kis Z, Maróti B, Szabó G (2015) Non-destructive analyses of bronze artefacts from Bronze Age Hungary using neutron-based methods. J Anal At Spectrom 30:685–693
2. Sessa C, Bagán H, Romero MT, García JF (2017) Effects of variability sources on analysis of the composition of large ancient metal objects. Microchem J 134:309–316
3. Giumlia-Mair A (2005) On surface analysis and archaeometallurgy. Nucl Instrum Methods B 239:35–43
4. Di Turo F, De Vito C, Coletti F, Mazzei F, Antiochia R, Favero G (2017) A multi-analytical approach for the validation of a jellified electrolyte: application to the study of ancient bronze patina. Michrochem J 134:154–163
5. Lutz J, Pernicka E (1996) energy dispersive X-ray fluorescence analysis of ancient copper alloys: empirical values for precision and accuracy. Archaeometry 38:313–323. https://doi.org/10.1111/j.1475-4754.1996.tb00779.x
6. Mödlinger M, Zs Kasztovszky, Kis Z, Maróti B, Kovács I, Szőkafalvi-Nagy Z, Gy Káli, Horváth E, Zs Sánta, El Morr Z (2014) Non-invasive PGAA, PIXE and ToF-ND analyses on Hungarian Bronze Age defensive armour. J Radioanal Nucl Chem 300:787–799
7. Oura Y, Saito A, Sueki K, Nakahara H, Tomizawa T, Nishikawa T, Yonezawa C, Matsue H, Sawahata H (1999) Prompt gamma-ray analysis of archaeological bronze. J Radioanal Nucl Chem 239:581–585
8. Molnár GL, Révay Z, Paul RL, Lindstrom RM (1998) Prompt-gamma activation analysis using the k_0 approach. J Radioanal Nucl Chem 234:21–26
9. Révay Z, Molnár GL (2003) Standardisation of the prompt gamma activation analysis method. Radiochim Acta 91:361–369
10. Révay Z, Firestone RB, Belgya T, Molnár GL (2004) Prompt gamma-ray spectrum catalog. In: Molnár GL (ed) Handbook of prompt gamma activation analysis with neutron beams. Springer, Boston, pp 173–364
11. Kasztovszky Z, Révay Z, Belgya T, Molnár GL (2000) Nondestructive analysis of metals by PGAA at the Budapest research reactor. J Radioanal Nucl Chem 244:379–382
12. Kasztovszky Z, Panczyk E, Fedorowicz W, Révay Z (2005) Comparative archaeometrical study of Roman silver coins by prompt gamma activation analysis and SEM-EDX. J Radioanal Nucl Chem 265:193–199
13. Maróti B, Szentmiklósi L, Belgya T (2016) Comparison of low-energy and coaxial HPGe detectors for prompt gamma activation analysis of metallic samples. J Radioanal Nucl Chem 310:743–749
14. Developments in prompt gamma-ray neutron activation analysis and cold neutron tomography and their application in non-destructive testing, Stefan Söllradl. Ph.D. dissertation, Universität Bern. https://pdfs.semanticscholar.org/a024/3960ee8b95cfc7e7c5fef574854ed544be44.pdf. Accessed 7 Aug 2017
15. Zs Révay, Kudějová P, Kleszcz K, Söllradl S, Genreith Ch (2015) In-beam activation analysis facility at MLZ, Garching. Nucl Instrum Methods A 799:114–123
16. Söllradl S, Lührs H, Zs Révay, Kudejova P, Canella L, Türler A (2013) Increasing the dynamic range for the analysis of boron in PGAA. J Radioanal Nucl Chem 298:2069–2073

17. Szentmiklósi L, Párkányi D, Sziklai-László I (2016) Upgrade of the Budapest neutron activation analysis laboratory. J Radioanal Nucl Chem 309:91–99

18. Constantinides I, Gritsch M, Adriaens A, Hutter H, Adams F (2001) Microstructural characterisation of five simulated archaeological copper alloys using light microscopy, scanning electron microscopy, energy dispersive X-ray microanalysis and secondary ion mass spectrometry. Anal Chim Acta 440:189–198

19. Bottaini C, Vilaca R, Schiavon N, Mirao J, Candeias A, Bordalo R, Paternoster G, Montero-Ruiz I (2016) New insights on Late Bronze Age Cu-metallurgy from Coles de Samuel hoard (central Portugal): a combined multi-analytical approach. J Archaeol Sci Rep 7:344–357

20. Charalambous A, Kassianidou V, Papasavvas G (2014) A compositional study of Cypriot bronzes dating to the Early Iron Age using portable X-ray fluorescence spectrometry (pXRF). J Archaeol Sci 46:205–216

21. Rehren Th, Boscher L, Pernicka E (2012) Large scale smelting of speiss and arsenical copper at Early Bronze Age Arisman, Iran. J Archaeol Sci 39:1717–1727

22. Ingelbrecht C, Adriaens A, Maier EA (2001) BCR information reference materials, The certification of As, Pb, Sn and Zn (mass fractions) in five copper alloys, Report EUR 19778/1 EN

23. Arana G, Wätjen U, Ingelbrecht C, Robouch P (2003) Bronze analysis by k_0-NAA and PIXE. J Radioanal Nucl Chem 257:603–608

24. Dungworth D (1997) Roman copper alloys: analysis of artefacts from northern Britain. J Archaeol Sci 24:901–910

25. Craddock PT (1978) The composition of the copper alloys used by the Greek, Etruscan and Roman civilizations. J Archaeol Sci 5:1–16

26. Lechtman H, Klein S (1999) The production of copper–arsenic alloys (Arsenic Bronze) by cosmelting: modern experiment, ancient practice. J Archaeol Sci 26:497–526

27. Merkl MB (2010) Bell Beaker metallurgy and the emergence of Fahlore-copper use in central Europe. Interdiscip Archaeol I:19–27

28. Czajlik Z (2012) A Kárpát-medence fémnyersanyag-forgalma a későbronzkorban és a vaskorban, Tálentum könyvek. ELTE BTK Régészettudományi Intézet, Budapest (in Hungarian). ISBN 9789632842783

29. Szentmiklósi L, Belgya T, Révay Z, Kis Z (2010) Upgrade of the prompt gamma activation analysis and the neutron-induced prompt gamma spectroscopy facilities at the Budapest research reactor. J Radioanal Nucl Chem 286:501–505

30. Heinz Maier-Leibnitz Zentrum, Révay Z (2015) PGAA: prompt gamma and in-beam neutron activation analysis facility. J Large Scale Res Facil 1:1–3. https://doi.org/10.17815/jlsrf-1-46

31. Fazekas B, Belgya T, Dabolczi L et al (1996) HYPERMET-PC: program for Automatic analysis of complex gamma-ray spectra. J Trace Microprobe Tech 14:167–172

32. Szentmiklósi L (2018) Fitting special peak shapes of prompt gamma spectra. J Radioanal Nucl Chem 315:663–670. https://doi.org/10.1007/s10967-017-5589-z

33. Revay Z (2009) Determining elemental composition using prompt gamma activation analysis. Anal Chem 81:6851–6859

34. Révay Z (2006) Calculation of uncertainties in prompt gamma activation analysis. Nucl Instrum Methods Phys Res A 564:688–697

35. Szentmiklosi L, Revay Z, Belgya T et al (2008) Combining prompt gamma activation analysis and off-line counting. J Radioanal Nucl Chem 278:657–660

36. 2015 edition of k_0 database. http://www.kayzero.com/k0naa/k0naaorg/Nuclear_Data_SC/Entries/2016/1/11_New_k0-data_Library_2015_files/k0_database_2015_12_04.xls. Accessed 20 Sept 2017

37. Kis Z, Szentmiklósi L, Belgya T et al (2015) Neutron based imaging and element-mapping at the Budapest Neutron Centre. Phys Proc 69:40–47

38. Jaćimović R, De Corte F, Kennedy G, Vermaercke P, Revay Z (2014) The 2012 recommended k_0 database. J Radioanal Nucl Chem 300:589–592

39. Simonits A, Ostor J, Kalvin S et al (2003) HyperLab: a new concept in gamma-ray spectrum analysis. J Radioanal Nucl Chem 257:589–595

40. De Corte F, Simonits A (1994) Vade Mecum for k0-Users, Addendum to the KAYZERO/SOLCOI software package. DSM Research, Gellen (NL), R94/11492, 25

41. Chilian C, Kennedy G (2012) Enhancement of thermal neutron self-shielding in materials surrounded by reflectors. J Radioanal Nucl Chem 293:179–183

42. Technical specifications—bAxil Software Package. http://www.brightspec.be/brightspec/downloads/bAXIL_Spec_V1.1_Extensive.pdf. Accessed 9 Oct 2017

43. Currie LA (1968) Limits for qualitative detection and quantitative determination. Anal Chem 40:586–593

44. Révay Z, Belgya T (2004) Principles of the PGAA method. In: Molnár GL (ed) Handbook of prompt gamma activation analysis with neutron beams. Springer, Boston, pp 1–30